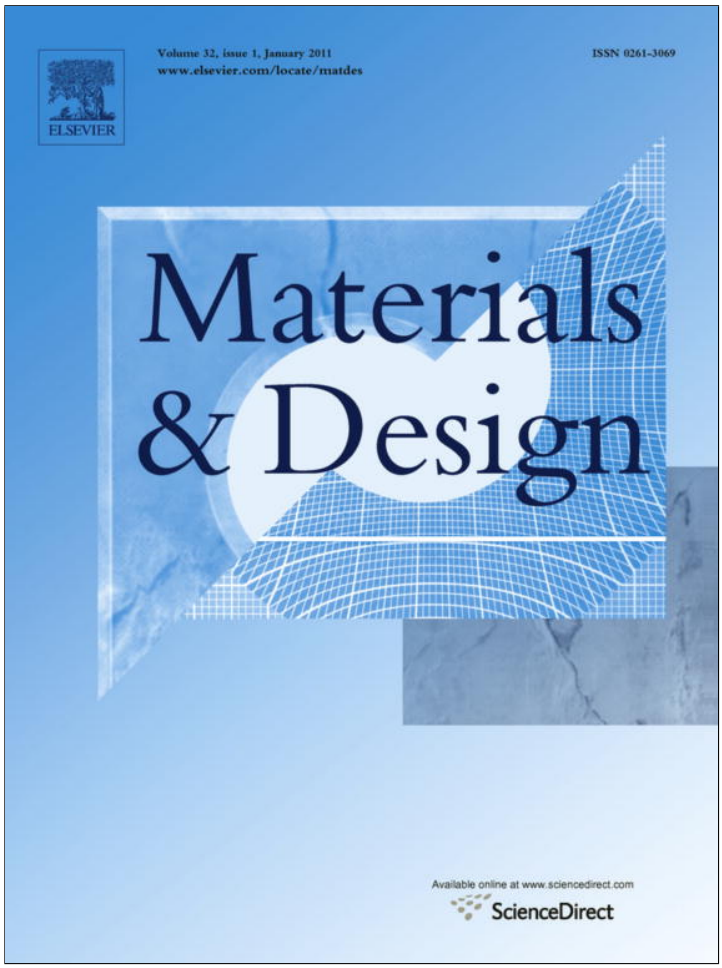


(This is a sample cover image for this issue. The actual cover is not yet available at this time.)

Materials and Design 33 (2012) 69–74

Contents lists available at ScienceDirect

Materials and Design

journal homepage: www.elsevier.com/locate/matdes

# Determination of local constitutive properties of aluminium friction stir welds using digital image correlation

C. Leitão, I. Galvão, R.M. Leal, D.M. Rodrigues *

*CEMUC, Department of Mechanical Engineering, University of Coimbra, Portugal*

ARTICLE INFO

*Article history:*
Received 6 May 2011
Accepted 4 July 2011
Available online 14 July 2011

*Keywords:*
Plastic behaviour
Welding
Aluminium alloys

ABSTRACT

In this paper a simple procedure for the characterization of the constitutive behaviour of welds is presented. Digital Image Correlation (DIC) is used for accessing local strain fields in transverse weld tensile samples and the stress distribution is calculated taking into account local strain data and thickness variation across the samples. The constitutive behaviour of the welds is assessed from local tensile stress–strain curves, plotted up to moderate values of plastic deformation, by fitting an appropriate work-hardening model to the experimental results and the ultimate tensile strength of the welds is estimated using the Considère criterion. Based on this information it is possible to assess the constitutive behaviour of different weld sub-zones, which cannot be derived from the hardness measurements, as well as evaluating the mis-match in yield stress and plastic properties across the welds. The proposed methodology is validated by comparing local stress–strain curves obtained by testing transverse weld samples of friction stir welds in very thin plates with those obtained by testing longitudinal samples of the same welds.



## 1. Introduction

It is well known that the global strength of any weld depends on the distribution of properties across the zones affected by the welding operation. Consequently, it is important to determine the local mechanical properties of different weld sub-zones in order to understand the global strength and ductility of the bonding. Mechanical characterization has traditionally been addressed by performing hardness tests across the welds, by testing miniature samples from each region of the weld or samples obtained by weld thermal simulation, and more recently, by using digital image correlation to obtain local stress–strain curves across transverse weld samples [1,2].

Hardness testing is the most well-known and widely used technique for the mechanical characterization of welds. However, no precise relations have yet been established to determine important constitutive relations, which enable the plastic behaviour of the welds to be described, from hardness data. Testing of miniature samples, from different weld sub-regions, allows constitutive properties to be determined [3–6]. However, the production and testing of such miniature specimens is very complicated. If steep gradients in material properties exist within the welds, then even very small specimens may exhibit non-homogeneous properties. This problem can be avoided by using bulk material samples from weld thermal simulation, which allows full-size specimens to be tested and properties from yield to fracture to be determined [7,8]. However, the highly transient thermal histories experienced by the welded joints are difficult to characterize accurately and to reproduce, which makes the use of thermal simulation samples simultaneously expensive and imprecise.

One important step towards the immediate characterization of the mechanical behaviour of different weld sub-zones and of the global response of the welds is the use of digital image correlation to obtain local and global stress–strain curves. Reynolds and Duvall [9] were pioneers in applying this technique to determine the constitutive behaviour of both weld and base metal constitutive behaviour. These authors, as well as all the others who have used this technique for the mechanical characterization of friction stir welds [10–12] and laser welds [13,14], assumed iso-stress conditions during transverse tensile weld sample loading. Using this assumption, the local stress–strain curves are determined by mapping the global applied stress to the corresponding local strain fields captured using DIC. Lockwood et al. [4] analysed the viability of the iso-stress assumption by performing numerical simulations of tensile tests, using a FE model replicating experimental welds with local material properties assessed by DIC. Full correspondence between predicted and measured global weld behaviour was not achieved, which was attributed to the possible limitations of the iso-stress load assumption in mechanical characterization.

Actually, assuming iso-stress conditions implies that the various weld regions are arranged in series and the cross-section at

* Corresponding author. Tel.: +351 239 790 700; fax: +351 239 790 701.
*E-mail address:* dulce.rodrigues@dem.uc.pt (D.M. Rodrigues).

0261-3069/$ - see front matter © 2011 Elsevier Ltd. All rights reserved.
doi:10.1016/j.matdes.2011.07.009

any location in the specimen is homogeneous [15]. However, this is not the case in welded samples for which, depending on the welding technology in use, steep microstructural gradients and thickness variations can be registered across the samples. In friction stir welding (FSW), for example, the forging action of the tool induces a significant thickness reduction in the weld relative to parent plate [16]. In the present study, the mechanical characterization of friction stir welds was performed using a very simple procedure which enabled local stress fields to be determined, by taking into account local thickness variations in the regions under evaluation and the local strain fields acquired by DIC. Since the stress and strain ranges in different sample regions are limited by the strength of the weakest region, the constitutive behaviour of the harder sample regions was assessed by fitting an appropriate hardening model to the "incomplete" stress–strain curves. This procedure enabled the local constitutive behaviour in different sample regions to be modelled as well as allowing the maximum strength in each weld region to be estimated using the Considère criterion.

## 2. Computation of local stress–strain curves from local strain fields

The methodology presented in this section enables local tensile stress–strain curves to be calculated from local strain fields registered using DIC during tensile tests of transverse weld specimens. Fig. 1a shows a schematic of a full-size transverse tensile specimen, with the weld centred in the gauge section and the loading axis normal to the welding direction. In this Fig. 1 indicates the weld, 2 the heat affected zone and 3 the base material. Fig. 1b shows an image of the major logarithmic strain ($\varepsilon_1$) distribution after maximum load, acquired using DIC, in a tensile sample. This clearly demonstrates the non-uniform strain distribution across the sample and the occurrence of rupture in the weld, where the largest strain values were registered.

Knowing the local strain values, the evolution of the cross sectional area of a specific part of the sample, $A^i$, can be determined using the following relationship

$$A^i = A_0^i \exp(-\varepsilon^i), \tag{1}$$

in which $A_0^i$ is the initial cross-section of the specimen in the zone under study, calculated after evaluating specimen dimensions across the samples, and $\varepsilon^i$ is the local axial strain registered using DIC.

The local stress in this area is obtained by dividing the applied load, $F$, by the actual cross sectional area, $A^i$, of the part of the sample under study:

$$\sigma^i = \frac{F}{A^i}. \tag{2}$$

Expressions (1) and (2) can be used as long as the sample part under analysis is subjected to uniaxial loading conditions. In order to evaluate if the local microstructural heterogeneities and geometric discontinuities across the transverse weld samples, such as thickness variations across the weld, had any influence on the local strain fields, the evolution of local principal logarithmic strains $\varepsilon_1^i$ versus $\varepsilon_2^i$ with plastic deformation should be analyzed before calculating the stress–strain curves. This analysis allows the occurrence of any local change of the deformation path during the tensile test to be determined. More precisely, it is possible to evaluate the existence of any local stress triaxiality and if it had any influence on the local stress–strain curves registered for each sample part.

## 3. Experimental procedure

Similar and dissimilar welds, obtained by friction stir welding of 1 mm thick aluminium sheets were tested in this study. The base materials were two very popular automotive aluminium alloys, AA5182-H111 (BM5) and AA6016-T4 (BM6) alloys. The welding conditions and results of the metallographic and mechanical analysis of the welds can be found in [17,18]. From these references it can be inferred that the AA5182 similar welds (S55) and the AA5182–AA6016 dissimilar welds (D56) were in over-match relative to the base material's hardness and yield stress, but the AA6016 similar welds (S66) were in under-match. Longitudinal and transverse samples were cut from all these welds, following the sampling scheme shown in Fig. 2.

In the present investigation, the tensile tests were performed in a 10 kN universal testing machine, operating at room temperature, with a nominal initial strain rate of $1.33 \times 10^{-3}\ s^{-1}$, in accordance with the ISO6892-1 standard [19]. The global strain of the longitudinal specimens (Fig. 2) was evaluated using a 50 mm gauge length clip-on extensometer. For the transverse samples, the local strain fields were determined by DIC using Aramis 3D 5M optical system (GOM GmbH). Before testing, the specimens were prepared by applying a random black speckle pattern, over the previously mat white painted surface of the transverse samples, in order to enable data acquisition by DIC. It is also important to clarify that none of the transverse or longitudinal samples were subjected to surface smoothing in order to homogenise sample thickness across the gauge section or avoid any influence from surface roughness on plastic behaviour.

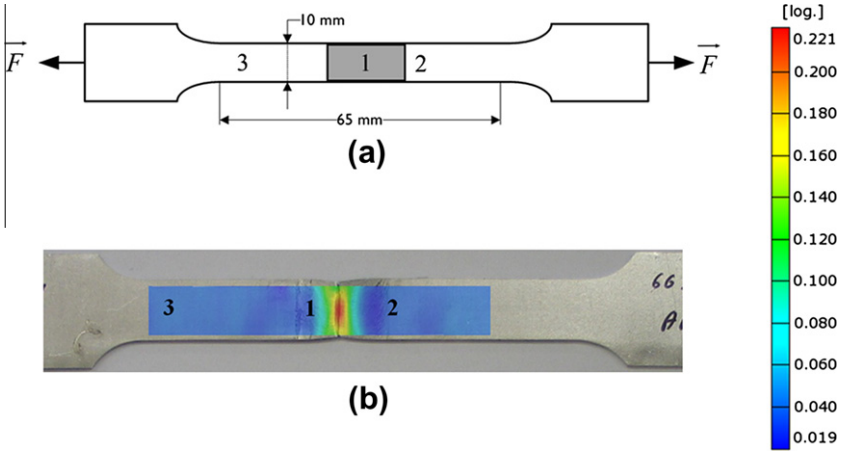


**Fig. 1.** Transverse tensile specimen: 1 – Weld; 2 – HAZ; 3 – BM.

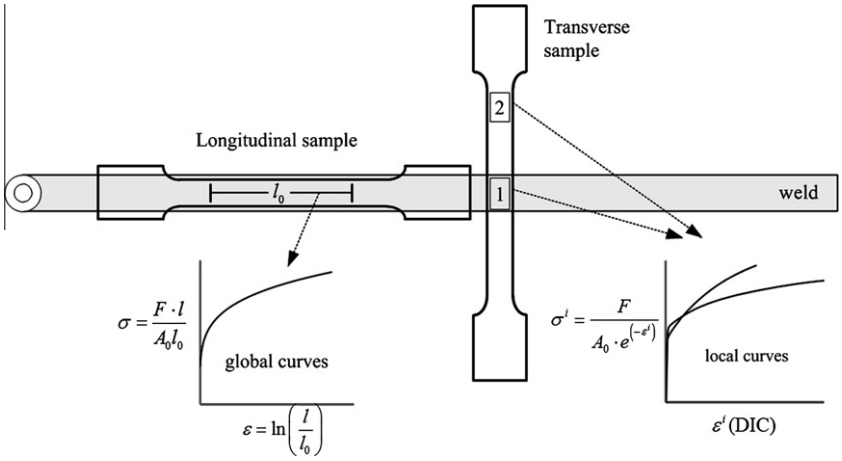


**Fig. 2.** Longitudinal and transverse tensile specimen scheme.

## 4. Results and discussion

In order to analyse the accuracy of the proposed methodology for evaluating the local mechanical behaviour of different specimen zones, the local stress–strain curves from tensile transverse weld specimens were plotted and compared with the global curves obtained from the tensile tests of longitudinal specimens, extracted from the same welds, as schematically shown in Fig. 2.

For each sample, local tensile stress–strain curves were calculated for sample regions corresponding to the weld (zone 1) and base material (zone 3) areas schematized in Fig. 1. Before computing the local cross-section area evolution, from Eq. (1), the local loading conditions were analysed by plotting the evolution of local principal logarithmic strains $\varepsilon_1^i$ against $\varepsilon_2^i$ with plastic deformation. The results obtained for the sample area corresponding to the weld, for all the specimens analysed in this investigation, are shown in Fig. 3. The logarithmic strain values plotted on this graph correspond to an average of the strain values registered for all the points located inside the areas under study, calculated using Aramis software [20]. The graph also shows the strain path corresponding to pure uniaxial loading conditions for isotropic materials ($\varepsilon_2 = -0.5\varepsilon_1$). By analysing the major and minor strain evolution in Fig. 3 it is possible to verify that linear strain paths were registered in the weld zone, for all the samples, before maximum load was attained. For the S66 and D56 samples, the deformation path started changing after maximum load had been attained (indicated in the figure by necking). For the samples of the overmatched S55 weld, necking occurred in the base material part of the samples and, for that reason, the strain path in the weld remained linear until the end of the test.

Comparing the strain paths corresponding to the welds, with those representing isotropic uniaxial loading conditions, it is possible to conclude that the slopes ($\varepsilon_1$ versus $\varepsilon_2$) corresponding to the welds strain paths are different from $-0.5$. This type of behaviour, which can be attributed to the existence of constraints in the deformed area and/or severe anisotropic conditions inside it, had no influence on mechanical characterization results, as will be shown in the next. Actually, in a previous numerical simulation study, Lockwood and Reynolds [15] established that the amount of constraint developed within the weld, during tensile loading, is primarily limited by specimen thickness. Tensile samples tested in current work were 1 mm thick, and for this reason constraint associated to thickness effects was expected to be very low.

In Fig. 4 the local stress–strain curves, for all the welds (S55,S66 and D56), obtained using Eqs. (1) and (2), and the global stress–strain curves (LONG5, LONG6 and LONG56), obtained by testing

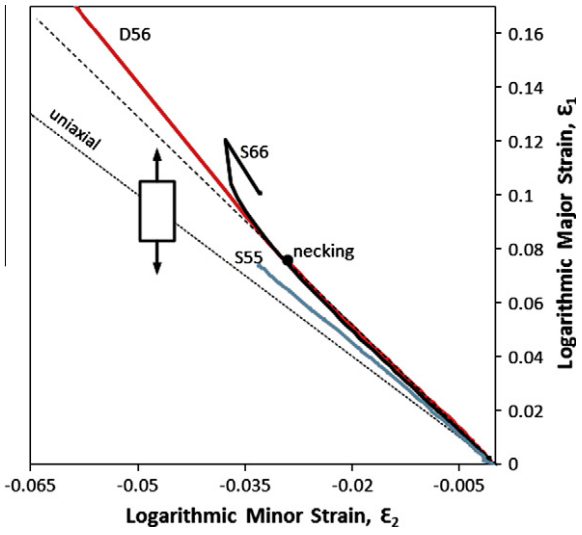


**Fig. 3.** Logarithmic major and minor strain evolution in the weld zone.

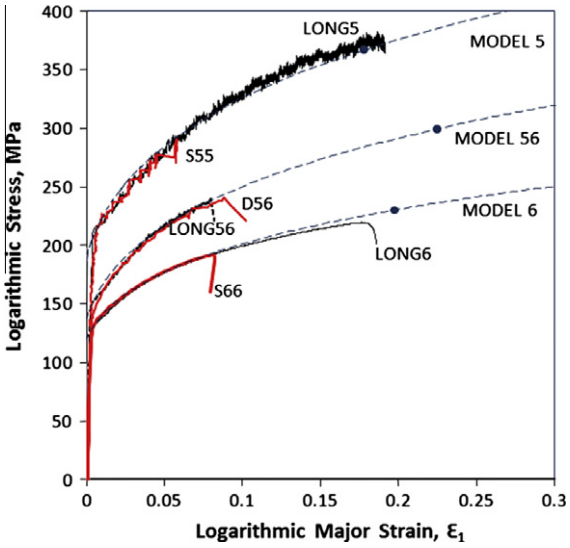


**Fig. 4.** Comparison of weld local strain–stress curves obtained by DIC and those corresponding to the longitudinal specimens.

longitudinal samples of each weld, are compared. This figure demonstrates that, for each weld, despite large differences in maximum strain levels, the local stress–strain curves overlap the stress–strain curves of the respective longitudinal samples. The large differences in strain at maximum load result from the strong heterogeneities in strain distribution across the transverse weld samples, as is shown in strain maps in Figs. 5–7, which correspond to two different periods during the tensile test: The right strain map in each figure corresponds to strain distribution at maximum load and the left strain map corresponds to strain distribution at an overall elongation of 50% of the elongation at maximum load. The non-homogeneous plastic deformation, which can be inferred from the strain maps, promoted local constraints that enforced premature strain localization in the transverse samples, relative to the homogeneous longitudinal samples. However, by comparing the local and longitudinal stress–strain curves in Fig. 4, for each weld, it is possible to conclude that these constraint effects had no strong influence on local loading conditions.

In order to predict the plastic behaviour of the welds up to high values of plastic deformation from the local tensile stress–strain curves, the Swift isotropic work-hardening model

$$\sigma = k(\varepsilon_0 + \bar{\varepsilon}^{\mathrm{p}})^n \tag{3}$$

was adjusted to the S55, S66 and D56 curves in Fig. 4. In this equation, $k$ and $\varepsilon_0$ are material constants, $\sigma$ is the flow stress in simple tension, $\bar{\varepsilon}^{\mathrm{p}}$ the equivalent plastic strain and $n$ the hardening coefficient. Material parameter identification was performed by using the in-house DD3MAT code [21]. The results are shown in Table 1 and the stress–strain curves, plotted according to Eq. (3), are shown in Fig. 4 (MODEL5, MODEL6 and MODEL56 curves). Table 1 shows the values of the ultimate tensile strength ($\sigma_{\mathrm{u}}$), for all the weld materials, estimated using the Considère criterion. According to this criterion, for the Swift equation:

$$\sigma_{\mathrm{u}} = kn^n \tag{4}$$

The maximum stress values, corresponding to each weld, are indicated by dots in the MODEL curves shown in the graph of Fig. 4. If the values predicted by the model are compared with the LONG curves results, it is possible to confirm the satisfactory quality of the predictions. In fact, major differences between experimental and model predictions, were only found for the dissimilar weld (D56), for which very small values of ultimate tensile strength were also registered from the tensile tests of the longitudinal samples. However, it is important to point out that the longitudinal samples had very irregular surface finishing, characteristic of friction stir weld crowns, which promoted non-uniform premature failure during the tensile test [17].

The curves plotted in Fig. 4 were computed using average strain values evaluated from the strain distribution inside the weld areas under measurement, which are indicated by rectangles in the strain maps in Figs. 5–7. However, in these strain maps, it is easy to distinguish easily the presence of strong heterogeneities in the plastic deformation across the welds. This plastic heterogeneity was evaluated by plotting local stress–strain curves, corresponding to different sub-zones inside each weld, which are identified by numbers 1 and 2 in the left strain maps.

The stress–strain results from the S55, S66 and D56 welds are shown in Figs. 5–7. In order to make it easy to understand the plastic heterogeneities inside the welds which can be inferred from the maps, the hardness profiles registered across the different welds were also added to the graphs. If the stress–strain curves and strain maps from the S55 weld (Fig. 5) are analysed, it is possible to observe that this weld is made up of two sub-zones with markedly different plastic behaviour (sub-zones 1 and 2). Although the two weld sub-zones display higher tensile strength than the base material (BM5 curve), it is possible to conclude that the central part of the weld (sub-zone 2) has improved mechanical properties relative to sub-zone 1, which corresponds to the retreating side of the weld. In the hardness profile plotted on the same graph it is also possible to see a progressive decrease in hardness from the centre of the weld to the base material on the retreating side of the weld. It is also interesting to note that the stress–strain curve from weld sub-zone 2 displays higher strength levels than those registered by testing longitudinal weld samples (LONG5, Fig. 4) or considering the average strain over the entire weld (S55 curve).

If the results from the S66 weld (Fig. 6) are examined, it is possible to conclude that despite the progressive gradient in properties at the retreating side of the weld, evident from the hardness profile, the plastic properties registered for sub-zones 1 and 2 of the S66 welds are not very different, both being very close to the plastic properties calculated considering the average strain over the entire weld area (S66). However, the stress–strain curve relative to sub-zone 1, at the retreating side of the weld, is closer to that of the S66 curve. Another important result is that, despite the decrease in hardness registered for the S66 welds, the yield stress registered for all the weld sub-zones is higher than that of the 6016-T4 base material (BM6 curve). However, since the base material displays stronger hardening with plastic deformation, its strength becomes higher than that of the weld for relatively small strain values.

If Fig. 7 is analysed, relative to the D56 welds, it is possible to observe strong gradients in plastic properties and hardness across

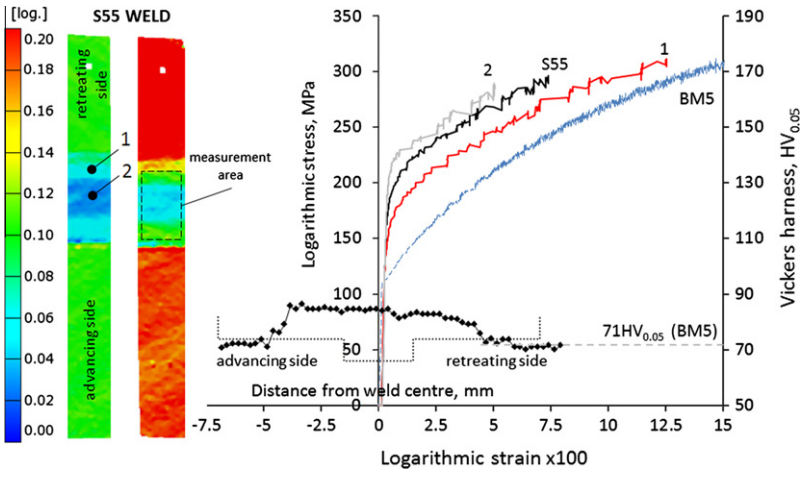


**Fig. 5.** Strain maps, stress–strain curves and hardness profile for the S55 weld.

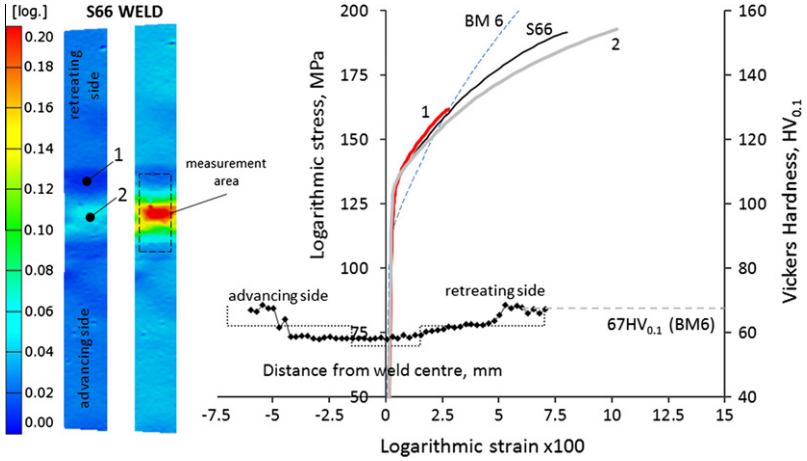


**Fig. 6.** Strain maps, stress–strain curves and hardness profile for the S66 weld.

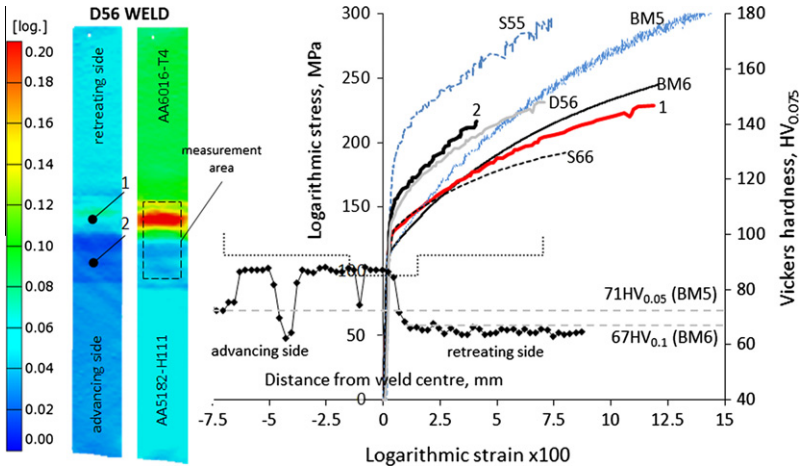


**Fig. 7.** Strain maps, stress–strain curves and hardness profile for the D56 weld.

**Table 1**
Swift coefficients for each curve and ultimate tensile strength ($\varepsilon_0 = 0.01$).

| | $k$ (MPa) | $n$ | $\sigma_u$ (MPa) |
|---|---|---|---|
| MODEL 5 | 520.1 | 0.222 | 372.5 |
| MODEL 6 | 319.8 | 0.210 | 230.6 |
| MODEL 56 | 420.0 | 0.233 | 299.1 |

the welds. For sub-zone 1, corresponding to the 6016-T4 side of the weld, where the hardness values registered are close to that of this base material, the stress–strain curve displays higher yield stress values but decreasing strength with plastic deformation, than the base material (BM6 curve). However, it is important to note that the mechanical properties in this sub-zone of the D56 welds are higher than those registered for the 6016-T4 similar welds (S66 curve) performed under the same welding conditions. Turning now to the results relative to the 5182-H111 (BM5) side of the weld, corresponding to sub-zone 2 in the strain map, it is possible to conclude that the local mechanical properties are higher than that of the base material here, but substantially lower than those registered for the 5182-H111 similar welds (S55 curve). This decrease in strength can be related to the strong local decrease in hardness registered on this side of the weld, which is evidenced by the hardness profile shown in the graph.

A deep characterization of local plastic heterogeneities inside the welds, as exemplified in the present investigation, is critical for the development of numerical models which can accurately predict the response of welds to various loading conditions. Several numerical studies have been devoted to modelling tailor welded blanks, with the aim of predicting forming behaviour [22], developing failure prediction models [23] or even analysing the impact of weld line modelling on numerical results [24,25]. These studies concluded that the implementation of weld details in the numerical models makes a significant contribution to the accuracy of the predictions. In the present study, local strain measurements, obtained from transversely loaded samples via DIC, enabled local stress fields to be calculated and the heterogeneity in plastic properties to be evaluated. Transverse tensile tests are simpler and quicker to perform than conventional hardness tests, which require a large number of time consuming measurements across the welds. They also provide an accurate evaluation of the constitutive behaviour of the different sub-zones of the welds, not available from the hardness measurements. Actually, in the present study, the yield stress values for the welds in hardness under-match were found to be higher than that of the corresponding base materials, which is not traditionally assumed. It was also demonstrated that it is possible to predict the plastic behaviour of the welds up to maximum load, from local tensile stress–strain curves plotted up to moderate values of plastic deformation, by adjusting an appropriate work-hardening model to the experimental results. It was even possible to estimate the ultimate tensile strength using the Considère criterion, allowing the achievement

of good quality previsions of the complete local tensile response for each zone.

## 5. Conclusions

The present results show the effectiveness of performing local plastic characterization of welds using digital image correlation (DIC):

- Local stress distribution was computed using strain data from tensile testing of transverse specimens.
- The constitutive behaviour of different weld regions was assessed from local tensile stress–strain curves.
- The ultimate tensile strength for all weld regions was estimated using the Considère criterion.

## Acknowledgments

The authors are indebted to the Portuguese Foundation for the Science and Technology (FCT) through COMPETE program from QREN and to FEDER for the financial support.

## References

[1] Lemmen HJK, Alderliesten RC, Benedictus R, Hofstede JCJ, Rodi R. The power of digital image correlation for detailed elastic–plastic strain measurements. In: WSEAS international conference on engineering mechanics, structures, engineering geology. Crate Island, Greece; 2008.
[2] Sutton MA, Yan JH, Avril S, Pierron F, Adeeb SM. Identification of heterogeneous constitutive parameters in a welded specimen: uniform stress and virtual fields methods for material property estimation. Exp Mech 2008;48:451–64.
[3] Amancio-Filho ST, Sheikhi S, dos Santos JF, Bolfarini C. Preliminary study on the microstructure and mechanical properties of dissimilar friction stir welds in aircraft aluminium alloys 2024-T351 and 6056-T4. J Mater Process Technol 2008;206:132–42.
[4] Lockwood WD, Tomaz B, Reynolds AP. Mechanical response of friction stir welded AA2024: experiment and modeling. Mater Sci Eng A 2002;323:348–53.
[5] Nielsen KL, Pardoen T, Tvergaard V, de Meester B, Simar A. Modelling of plastic flow localisation and damage development in friction stir welded 6005 A aluminium alloy using physics based strain hardening law. Int J Solids Struct 2010;47:2359–70.
[6] Molak RM, Paradowski K, Brynk T, Ciupinski L, Pakiela Z, Kurzydlowski KJ. Measurement of mechanical properties in a 316 L stainless steel welded joint. Int J Press Vessels Pip 2009;86:43–7.
[7] Bleck W, Reisgen U, Mokrov O, Rossiter E, Rieger T. Methodology for thermomechanical simulation and validation of mechanical weld-seam properties. Adv Eng Mater 2010;12:147–52.
[8] Zhang ZL, Silvanus J, Li HK, Shi QY. Sensitivity analysis of history dependent material mechanical models for numerical simulation of welding process. Sci Technol Weld Joi 2008;13:422–9.
[9] Reynolds AP, Duvall F. Digital image correlation for determination of weld and base metal constitutive behavior. Weld J 1999;78:355S–60S.
[10] Genevois C, Deschamps A, Vacher P. Comparative study on local and global mechanical properties of 2024 T351, 2024 T6 and 5251 O friction stir welds. Mater Sci Eng A – Struct 2006;415:162–70.
[11] Hatamleh O. Effects of peening on mechanical properties in friction stir welded 2195 aluminum alloy joints. Mater Sci Eng A 2008;492:168–76.
[12] Brown R, Tang W, Reynolds AP. Multi-pass friction stir welding in alloy 7050-T7451: effects on weld response variables and on weld properties. Mater Sci Eng A 2009;513–514:115–21.
[13] Boyce B, Reu P, Robino C. The constitutive behavior of laser welds in 304 L stainless steel determined by digital image correlation. Metall Mater Trans A 2006;37:2481–92.
[14] Scintilla LD, Tricarico L, Brandizzi M, Satriano AA. Nd:YAG laser weldability and mechanical properties of AZ31 magnesium alloy butt joints. J Mater Process Technol 2010;210:2206–14.
[15] Lockwood WD, Reynolds AP. Simulation of the global response of a friction stir weld using local constitutive behavior. Mater Sci Eng A 2003;339:35–42.
[16] Louro R, Leitao C, Puehringer T, Gouveia H, Loureiro A, Rodrigues DM. The relation between the plunge pressure and the mechanical properties of friction stir welded 3 mm thick AA6082-T651 Sheets. Mater Sci Forum 2010;636–637:578–84.
[17] Leitao C, Leal RM, Rodrigues DM, Loureiro A, Vilaça P. Mechanical behaviour of similar and dissimilar AA5182-H111 and AA6016-T4 thin friction stir welds. Mater Des 2009;30:101–8.
[18] Leal RM, Leitão C, Loureiro A, Rodrigues DM, Vilaça P. Material flow in heterogeneous friction stir welding of thin aluminium sheets: effect of shoulder geometry. Mater Sci Eng A 2008;498:384–91.
[19] ISO 6892-1:2009. Metallic materials – tensile testing – part1: method of test at room temperature.
[20] Gom.com. Braunschweig: GOM – optical measurement techniques, GmbH; 2011. <http://www.gom.com/home.html>.
[21] Chaparro BM, Thuillier S, Menezes LF, Manach PY, Fernandes JV. Material parameters identification: Gradient-based, genetic and hybrid optimization algorithms. Comput Mater Sci 2008;44:339–46.
[22] Veera Babu K, Ganesh Narayanan R, Saravana Kumar G. An expert system for predicting the deep drawing behavior of tailor welded blanks. Expert Syst Appl 2010;37:7802–12.
[23] Zadpoor AA, Sinke J, Benedictus R. Finite element modeling and failure prediction of friction stir welded blanks. Mater Des 2009;30:1423–34.
[24] Raymond SD, Wild PM, Bayley CJ. On modeling of the weld line in finite element analyses of tailor-welded blank forming operations. J Mater Process Technol 2004;147:28–37.
[25] Shi Y, Lin Z, Zhu P, Han S. Impact modeling of the weld line of tailor-welded blank. Mater Des 2008;29:232–8.